Applied Physics Letters

Formation of γ-Ga_2O_3 by ion implantation: Polymorphic phase transformation of β-Ga_2O_3

Cite as: Appl. Phys. Lett. **121**, 191601 (2022); https://doi.org/10.1063/5.0120103
Submitted: 11 August 2022 • Accepted: 20 October 2022 • Published Online: 07 November 2022

J. García-Fernández, S. B. Kjeldby, P. D. Nguyen, et al.

AIP Publishing

Applied Physics Letters ARTICLE scitation.org/journal/apl

Formation of γ-Ga_2O_3 by ion implantation: Polymorphic phase transformation of β-Ga_2O_3

Cite as: Appl. Phys. Lett. **121**, 191601 (2022); doi: 10.1063/5.0120103
Submitted: 11 August 2022 · Accepted: 20 October 2022 ·
Published Online: 7 November 2022

J. García-Fernández,[a] S. B. Kjeldby, P. D. Nguyen, O. B. Karlsen, L. Vines, and Ø. Prytz[a]

AFFILIATIONS

Department of Physics and Center for Materials Science and Nanotechnology, University of Oslo, Oslo 0315, Norway

[a]**Authors to whom correspondence should be addressed:** j.g.fernandez@smn.uio.no and oystein.prytz@fys.uio.no

ABSTRACT

Ion implantation induced phase transformation and the crystal structure of a series of ion implanted β-Ga_2O_3 samples were studied using electron diffraction, high resolution transmission electron microscopy, and scanning transmission electron microscopy. In contrast to previous reports suggesting an ion implantation induced transformation to the orthorhombic κ-phase, we show that for $^{28}Si^+$, $^{58}Ni^+$, and stoichiometric $^{69}Ga^+/^{16}O^+$-implantations, the monoclinic β-phase transforms to the cubic γ-phase. The γ-phase was confirmed for implantations over a range of fluences from 10^{14} to 10^{16} ions/cm^2, indicating that the transformation is a general phenomenon for β-Ga_2O_3 due to strain accumulation and/or γ-Ga_2O_3 being energetically preferred over highly defective β-Ga_2O_3.

Gallium sesquioxide, Ga_2O_3, which can exist in several polymorphic forms, has attracted considerable attention in the last few years due to its potential applications for power electronics and UV devices.[1,2] The monoclinic β-phase (β-Ga_2O_3) is the thermodynamically stable polymorph at room temperature and atmospheric pressure in air,[3] but other polymorphs also display attractive properties and can be stabilized using soft chemical synthesis methods,[4] high temperature and high pressure solid state synthesis,[5] strain engineering in thin films,[6] or ion implantation.[7] For example, the orthorhombic κ-phase may exhibit spontaneous polarization,[8] while nanoparticles of the cubic defective spinel γ-phase can be suitable for catalyst uses.[9] The other known polymorphs, the rhombohedral α-phase, and the cubic δ-phase also exhibit attractive features for solar-blind UV detection applications or MIS diodes with a high breakdown voltage.[10,11]

Ion implantation produces complex changes in the microstructure of the exposed material. It can lead to disorder, formation of secondary phases in the form of nanoscale inclusions[12,13] and, for sufficiently high fluences, amorphization commonly occurs.[14,15] Recently, it was shown that ion implantation of bulk β-Ga_2O_3 samples could lead to a polymorphic transformation, forming a continuous, although defective layer.[7,16] This intriguing observation may open up possibilities to stabilize metastable polymorphs on top of bulk β-Ga_2O_3, forming either an active layer or acting as a template for further growth. The polymorphic transformation is noteworthy, since high-fluence ion implantations normally yield amorphization in the implanted material. However, β-Ga_2O_3 is not unique in displaying such transformations. In fact, similar effects occur in ZrO_2,[17,18] HfO_2,[19,20] Cu_2O/CuO,[21] GaN nanowires,[22] TiO_2,[23] and Co nanoparticles.[24]

Anber *et al.*,[7] and later Azarov *et al.*,[16] reported on the formation of κ-phase after implantation with Ge, Ni, Ga, and Au ions in β-Ga_2O_3. The proposed assignment of the κ-phase was based on selected area electron diffraction (SAED) patterns obtained by transmission electron microscopy (TEM). However, no SAED or high-resolution TEM or scanning TEM (HRTEM/STEM) images could unambiguously confirm the κ-phase. Here, we propose an alternative assignment of the phase transformed layer by indexing it as the γ-phase. γ-Ga_2O_3 has a defective cubic spinel structure with the space group *Fd-3m* (227), a lattice parameter of $a = 8.23$ Å, with gallium being tetrahedrally and octahedrally coordinated to oxygen atoms.[25] This metastable γ-phase has attracted appreciable attention as its physical and chemical properties, such as wide band gap (~4.7 eV), are of interest for diverse applications including photonics (ultraviolet photodetectors), solar devices, and photocatalysis.[26–28] A detailed investigation of the γ-phase by STEM was conducted by Yoo *et al.*[29] discovering that Sn ion implantation induces the phase transformation from the β-phase to the γ-phase with high density of defects.

In the present work, we have carefully evaluated the structural evolution and phase transformations of $(\bar{2}01)$ and (010) oriented β-Ga_2O_3 implanted with $^{28}Si^+$, $^{58}Ni^+$, and $^{69}Ga^+/^{16}O^+$ ions using SAED and HRTEM and STEM imaging. We have implanted with $^{28}Si^+$, since it is an effective donor dopant in Ga_2O_3.[30,31] $^{69}Ga^+/^{16}O^+$ and $^{58}Ni^+$ implantations are used to evaluate the influence of the implanted ion

and to relate our work to previous reports.[7,16] The SAED patterns combined with HRTEM and STEM images unambiguously show a phase transition from β-Ga_2O_3 to γ-Ga_2O_3 which is independent of the implanted species.

Ion implantations of $(\bar{2}01)$ oriented β-Ga_2O_3 single crystal wafers were performed in an NEC Tandem Accelerator. All samples were implanted at room temperature and at 7° from the surface normal. ^{28}Si-implantation was performed with a fluence of 1×10^{14} Si/cm^2 and 1×10^{15} Si/cm^2 at an energy of 300 keV. An additional ^{28}Si-implantation was performed in (010) oriented β-Ga_2O_3 single crystal wafers with a fluence of 2×10^{16} Si/cm^2 and at the same energy. Detailed characterizations by x-ray diffraction (XRD) and Rutherford backscattering spectrometry in the channeling mode on these samples were performed in our previous work.[32] For the stoichiometric implantation, the energies of $^{69}Ga^+$ and $^{16}O^+$ ions were selected to achieve the same projected range as for the Si-ions, yielding implantation energies of 715 keV for $^{69}Ga^+$ and 182 keV for $^{16}O^+$. The ratio of $^{69}Ga^+$ and $^{16}O^+$ fluences was fixed at 2/3, to match the stoichiometry of the sample. The total implantation fluency was selected to obtain the same number of defects at the defect peak for $^{28}Si^+$ and stoichiometric implantation, this means fluence values of 2.85×10^{14} Ga/cm^2 and 4.28×10^{14} O/cm^2. For $^{58}Ni^+$-implantation, we used an implantation energy of 400 keV and a fluence of 1×10^{15} Ni/cm^2 in order to correlate our work to previous reports on phase transformation in β-Ga_2O_3 after ion implantation.[16]

Electron transparent cross-sectional TEM samples were prepared by mechanical grinding, polishing, and final thinning by Ar ion milling in a Gatan PIPS II (Model 695). Plasma cleaning (Fishione Model 1020) was applied immediately prior to the TEM investigations. A JEOL JEM-2100F microscope operated at an acceleration voltage of 200 kV was used for initial sample investigations using SAED and HRTEM. Additionally, SAED and HRSTEM imaging were conducted using a Thermo Fisher Scientific Cs-corrected Titan G2 60–300 kV microscope operated at 300 kV. High angle annular dark field (HAADF) STEM images were recorded using a probe convergence semi-angle of 23 mrad, a nominal camera length of 60 mm, corresponding to an inner and outer collection semi-angle of 100 and 200 mrad, respectively. Annular bright field (ABF) STEM images were simultaneously acquired at the same camera length, with collection semi-angles of 10 and 20 mrad. SAED simulations were performed using the JEMS software package[33]

Starting with the Ni-implantation, the implantation parameters were similar to those used in previous work by Azarov *et al.*,[16] where the κ-phase was reported. Contrary to the previous work, our results show that the transformed layer is γ-phase rather than κ-phase. We base this on the SAED patterns shown in Figs. 1(a)–1(c). These patterns are fully indexed as γ-phase (space group *Fd-3m*, lattice parameter $a = 8.36(2)$ Å) observed along the [110], [111], and [112] zone axes, respectively. The measured interplanar distances are shown in Table S1 of the supplementary material. Our lattice parameter is slightly higher than reported previously.[25] If this is a real feature of the sample, it may be a consequence of implantation-induced strain.

Looking closely at the SAED patterns reported by Anber *et al.*[7] and Azarov *et al.*,[16] we believe that the pattern indexed as [001] zone axis of κ-phase is actually the γ-phase along the [111] zone axis. These results shed a new light by confirming that the transformation that occurs is from the β-phase to the γ-phase, in good agreement with recent reports by Yoo *et al.*[29] In order to confirm this, we have performed simulations of κ-Ga_2O_3 along [001] zone axis, a superposition of 3 SAEDs of κ-Ga_2O_3 [001] rotated 120° as reported by Cora *et al.*[34] as a consequence of twinning resulting in a diffraction pattern with sixfold symmetry, and a simulated SAED of the γ-Ga_2O_3 phase along [111] zone axis. All these simulated SAEDs are shown in the supplementary material [Figs. S1(a)–S1(c)] together with the experimental SAED of γ-Ga_2O_3 phase along [111] zone axis in Fig. 1(b) [Fig. S1(d)] for better comparison. As can be seen, there is a close agreement between our experimental SAED and the simulated one for γ-Ga_2O_3.

For Si-implantation, XRD showed that for the samples implanted with 1×10^{14} Si/cm^2 only small peaks and shoulders attributed to the implantation-induced strain were observed, as reported previously.[32] However, SAED pattern recorded at the top area of the sample [Fig. S2(a) in the supplementary material] along the [102] zone axis of β-phase shows the presence of an extra weak and diffuse contrast (indicated by blue arrows) where the $(\bar{2}20)$ plane of the γ-phase along the [112] zone axis should be [see Fig. 1(c) for a γ-phase SAED in this projection]. Figure S2(b) in the supplementary material shows an intensity profile along the line marked with yellow dashed dots in Fig. S2(a) for a better visualization. This intensity could indicate the presence of a very small fraction of γ-Ga_2O_3 (and, thus, the beginning of the transformation) in the sample, which was undetectable by XRD. For the fluences of 1×10^{15} Si/cm^2 and above, new XRD peaks were observed and HRTEM showed that the upper 400 nm of the sample had transformed. Here, we also find that the upper 400 nm of the samples has undergone a change in the crystal structure. Henceforth, we call this layer the transformed layer. Similar observations are made for all of the implanted samples in this work. Figure 2(a) shows a TEM

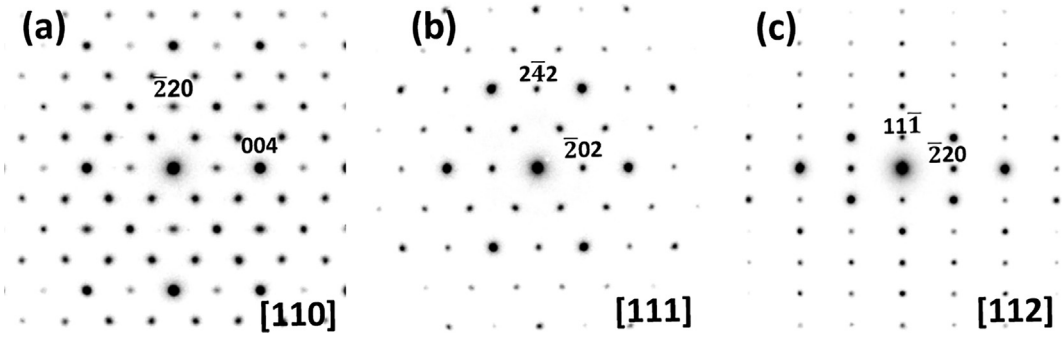

FIG. 1. SAED pattern from the transformed layer of the Ni implanted sample. The indexing is according to γ-Ga_2O_3 along the zone axes (a) [110], (b) [111], and (c) [112].

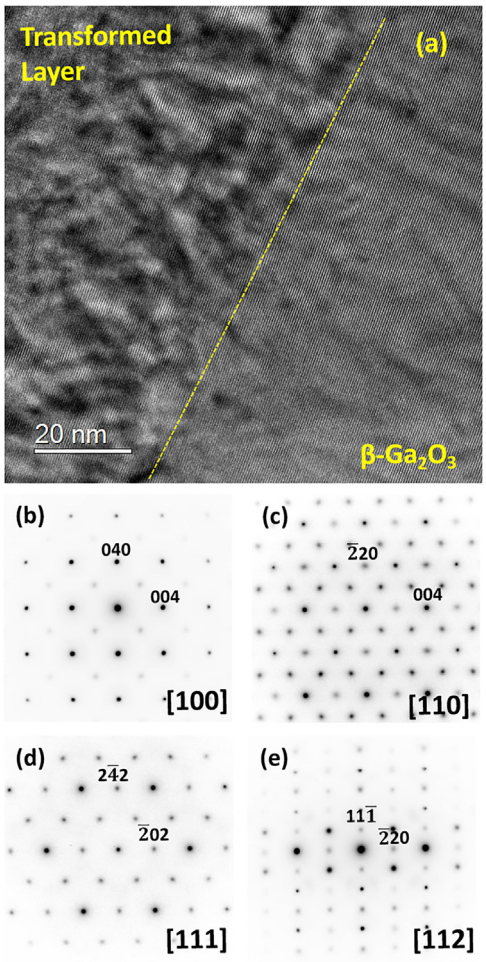

FIG. 2. (a) Cross-sectional TEM image of the interface between the transformed layer and the $(\bar{2}01)$ oriented β-Ga_2O_3 of the Si-implanted sample. SAED pattern of the transformed layer indexed according to γ-Ga_2O_3 along the zone axes (b) [100], (c) [110], (d) [111], and (e) [112].

image of the interface between the $(\bar{2}01)$ oriented β-Ga_2O_3 and the transformed layer in the sample implanted with 1×10^{15} Si/cm^2. The difference in contrast due to defects and strain in the transformed layer compared with the β-Ga_2O_3 below is clearly observed in the image. This corroborates that strain and defect formation are part of the structural transition mechanism. Figures 2(b)–2(e) show the SAED patterns from the transformed layer in various projections. The SAED pattern along [100] zone axis [Fig. 2(b)] is acquired from the (010) oriented β-Ga_2O_3 sample, and the others are from the $(\bar{2}01)$ oriented β-Ga_2O_3 sample. All the SAED patterns from the two samples can be indexed unambiguously as γ-Ga_2O_3, indicating that the orientation of the β-Ga_2O_3 does not have any influence on the phase transformation.

It is important to note that in the SAED patterns published by Anber *et al.*[7] and Azarov *et al.*,[16] some diffuse spots are observed. If we enhance the contrast of the SAED pattern in Fig. 2(d), similar diffuse spots become visible in our data, as shown in Fig. 3(a) and marked by orange arrows. For comparison, Fig. 3(b) is a SAED pattern taken at

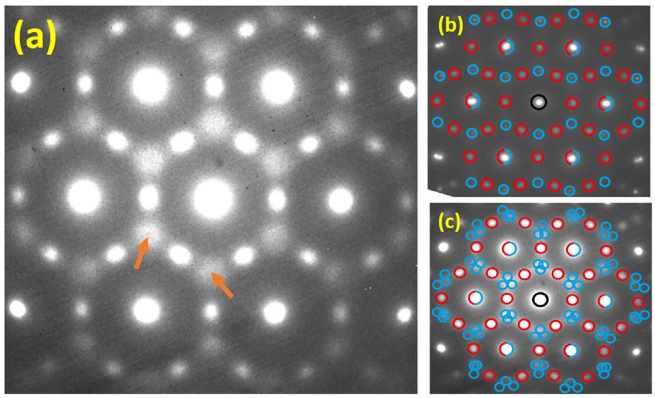

FIG. 3. (a) SAED pattern from the sample implanted with 1×10^{15} Si/cm^2 taken along the [111] zone axis. This is the same pattern shown in Fig. 2(d) but has been digitally modified to reveal weak diffuse spots (two of them marked with orange arrows) that cannot be explained by the γ-phase. (b) SAED pattern from the interface, showing diffraction spots from both the β-phase (blue circles) and the γ-phase (red circles). (c) Superimposing three of the traced patterns, each rotated 120°, onto (a) shows that each diffuse spot is surrounded by three small, blue circles.

the interface, showing diffraction spots from both the transformed and untransformed layer. All spots have been marked with circles. The diffuse spots in Fig. 3(a) are indeed close to the position of the β-spots that are not overlapping with those from the γ-spots, but the arrangement has lower symmetry than the sixfold rotational symmetry of the [111] projection of the γ-phase. If we superimpose three of the traced blue patterns in Fig. 3(b), each rotated 120°, the diffuse spots are closely surrounded by three of the spots from the β-phase [see Fig. 3(c)]. We, therefore, boldly propose that the diffuse spots originate from very small precipitates of the β-phase inside the γ-phase. The three orientations would be expected if the orientation of the β-phase is dictated by the threefold symmetry of the γ-phase. Although we have not observed these inclusions in the HRTEM or STEM imaging, such a reversion of γ-phase to β-phase should not be surprising. The β-phase is the thermodynamically stable polymorph at ambient conditions, and we have earlier shown that the γ-phase converts to β-phase during annealing.[32]

The atomic structures of the polymorphs were also studied by atomic-resolution STEM imaging. Figure 4(a) shows an HAADF STEM image of the interface between the β-Ga_2O_3 (displayed along the [102] zone axis) and the transformed layer (along the [112] zone axis). Figures 4(b) and 4(c) show representative simultaneously acquired HAADF and ABF STEM images along the [112] zone axis of the γ-phase, respectively. In the HAADF image, the brighter spots are associated with the arrangement of the heavy gallium cations in the γ-phase. In the ABF image, the locations of both gallium and oxygen atoms are identified as dark spots over a white background. The atomic arrangement of gallium (orange) and oxygen (blue) atoms are schematically represented. The gallium atoms in the positions corresponding to Wyckoff site 8a (T_d) and 16d (O_h) in the ideal spinel structure are clearly visible and marked in the insets of Figs. 4(b) and 4(c). However, according to the structure reported by Playford *et al.*[25] using neutron diffraction, two more gallium positions are needed to get a proper refinement of the diffractogram. These extra atomic positions are placed in 48f (T_d) and 16c (O_h). In our images, the contrast

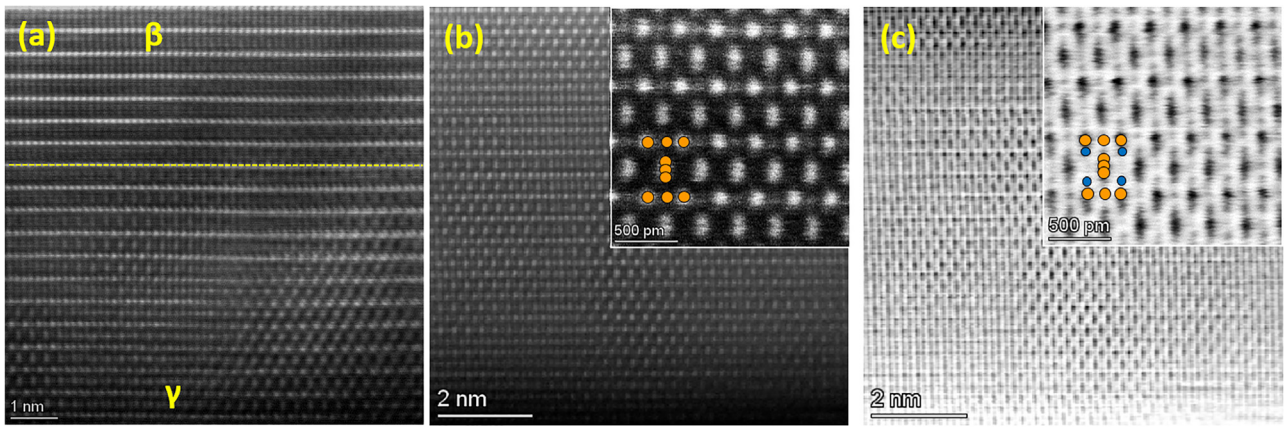

FIG. 4. (a) Atomic resolution HAADF STEM image of the interface between β-Ga_2O_3 (along [102] zone axis) and γ-Ga_2O_3 (along [112] zone axis) of the 1×10^{15} Si/cm^2 sample. (b) and (c) show HAADF and ABF STEM image of γ-Ga_2O_3 along [112] zone axis, respectively. The insets show areas at higher magnification. Gallium and oxygen atoms are schematically represented in orange and blue, respectively.

from these atomic columns is not resolved. This is as expected due to the low occupancy of both positions: 0.066 and 0.024, respectively. Our own experimental observations are in good agreement with the γ-phase structure analysis by electron microscopy reported by Cora *et al.*[35] and Castro-Fernandez *et al.*[36] when observed along the same zone axis.

In order to study the effect of chemical factors specific to the implanted ion on the phase transformation, a $(\bar{2}01)$ oriented β-Ga_2O_3 sample was implanted with $^{69}Ga^+/^{16}O^+$ in the stoichiometric ratio. Ion implantation parameters were selected to give projected range and defect generation similar to the Si-implantation. Figures 5(a) and 5(b) show the SAED patterns and representative HAADF STEM images of the transformed layer corresponding to the [112] and [111] zone axes of the γ-Ga_2O_3 phase, respectively. In both images, the positions of gallium atomic columns are marked in orange.

Diffraction patterns acquired for multiple zone axes and multiple implanted species clearly show that it is the γ-phase that is formed in this implantation-induced phase transformation. The formation of γ-Ga_2O_3 is also independent of the orientation of the implanted β-Ga_2O_3 wafers. This indicates that the transformation and stabilization by ion implantation is not driven by the chemistry of the implanted ions, and also not by factors such as the ionic size of the implanted species, since the transformation occurred even for stoichiometric implantation.

Azarov *et al.*[16] have previously interpreted phase transitions in ion implanted β-Ga_2O_3 as a direct consequence of strain accumulation. Although the present work shows that it is the γ-phase rather than the κ-phase which is formed, we cannot rule out contributions from strain in the transformation mechanism. Another possible mechanism behind the transformation might be that defect-rich γ-Ga_2O_3 could be energetically preferred over defect-rich β-Ga_2O_3, even though the β-phase is preferred for low defect concentrations.[37] We note that the energy transferred to the sample during implantation is highly localized and that it could, therefore, be difficult to drive transformations which require long-range transport, such as precipitations of phases with different crystal structures. We further find that the anion sublattice stacking sequence is mostly conserved in the β-to-γ

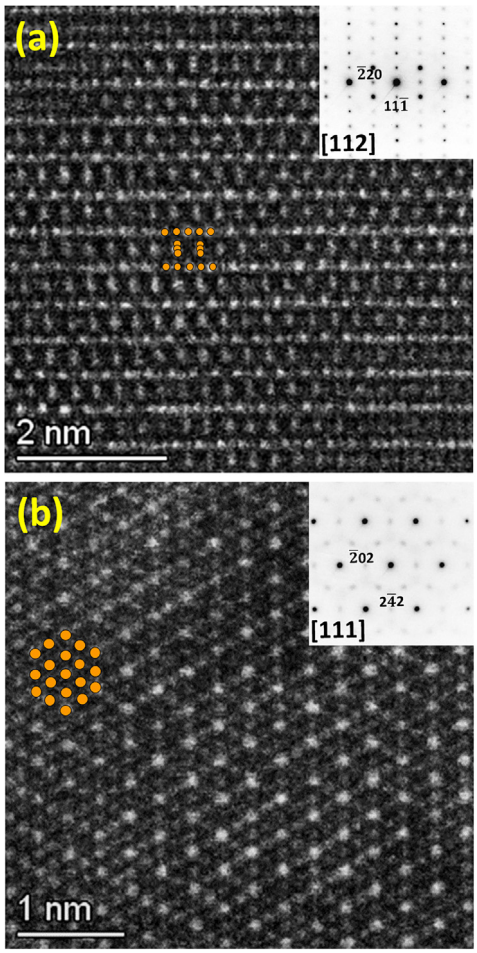

FIG. 5. SAED pattern and atomic resolution HAADF STEM images of the $^{69}Ga^+/^{16}O^+$ implanted sample along the zone axes (a) [112] and (b) [111]. Gallium is schematically represented in orange in both images.

transformation, while it would not be conserved in a β-to-κ transformation. To illustrate this, a schematic representation of the oxygen sublattice of β-Ga_2O_3 and γ-Ga_2O_3 at the interface is shown in Fig. S3 in the supplementary material, along with a schematic representation of the potential interface between β-Ga_2O_3 and κ-Ga_2O_3 for comparison. This structural similarity of the initial and final crystal structures could lower the transition energy for transformation to the γ-phase, promoting transformation to this phase rather than the κ-phase. This warrants a thorough investigation of the structural stability and mechanism of why and how γ-Ga_2O_3 has been stabilized but this is considered outside the scope of the present study.

In summary, we have systematically investigated the structural evolution of β-Ga_2O_3 implanted with $^{28}Si^+$, $^{58}Ni^+$, and $^{69}Ga^+/^{16}O^+$ ions using SAED and HRTEM/STEM over a range of fluences from 10^{14} to 10^{16} ions/cm^2 in surface orientations $(\bar{2}01)$ and (010). We demonstrate that the ion implantations resulted in β- to γ-polymorphic phase transformation. This process occurred independently of the investigated implanted species, which suggests that the transformation is an intrinsic feature of the implantation and is likely unrelated to chemical effects. This opens up the possibility of designing new devices and applications through customized "polymorph engineering" in thin films and interfaces.

See the supplementary material for some interplanar distances for the Ni implanted sample; SAED simulations of κ-Ga_2O_3 along [001] zone axis, a superposition of three SAEDs of κ-Ga_2O_3 along [001] zone axis rotated 120° as a consequence of twinning and γ-Ga_2O_3 along [111] zone axis; SAED analysis of the sample implanted with 1×10^{14} Si/cm^2; and schematic representation of the oxygen sublattice of β-Ga_2O_3 and γ-Ga_2O_3 or κ-Ga_2O_3 along the interface.

The Research Council of Norway is acknowledged for the support to the Norwegian Center for Transmission Electron Microscopy (NORTEM, No. 197405/F50), the Norwegian Micro- and Nanofabrication Facility (NorFab, No. 295864), and the NANO2021 researcher project Functionalization of conducting oxides by ion beam and defect engineering (FUNCTION, No. 287729).

AUTHOR DECLARATIONS

Conflict of Interest

The authors have no conflicts to disclose.

Author Contributions

Javier García-Fernández: Conceptualization (equal); Data curation (equal); Formal analysis (equal); Investigation (equal); Methodology (equal); Writing – original draft (equal). **Snorre Braathen Kjeldby:** Conceptualization (equal); Data curation (equal); Formal analysis (equal); Investigation (equal); Methodology (equal); Visualization (equal); Writing – original draft (equal). **Phuong Dan Nguyen:** Conceptualization (equal); Formal analysis (equal); Methodology (equal); Supervision (equal); Validation (equal); Writing – original draft (equal); Writing – review & editing (equal). **Ole Bjørn Karlsen:** Conceptualization (equal); Formal analysis (equal); Investigation (equal); Project administration (equal); Supervision (equal); Writing – original draft (equal); Writing – review & editing (equal). **Lasse Vines:** Investigation (equal); Resources (equal); Supervision (equal); Validation (equal); Visualization (equal); Writing – review & editing (equal). **Øystein Prytz:** Project administration (equal); Supervision (equal); Validation (equal); Writing – review & editing (equal).

DATA AVAILABILITY

The data that support the findings of this study are available from the corresponding authors upon reasonable request.

REFERENCES

[1]R. Singh, T. R. Lenka, D. K. Panda, R. T. Velpula, B. Jain, H. Q. T. Bui, and H. P. T. Nguyen, Mater. Sci. Semicond. Process. **119**, 105216 (2020).
[2]M. Zhong, Z. Wei, X. Meng, F. Wu, and J. Li, J. Alloys Compd. **619**, 572 (2015).
[3]M. Zinkevich and F. Aldinger, J. Am. Ceram. Soc. **87**, 683 (2004).
[4]T. Wang, S. S. Farvid, M. Abulikemu, and P. V. Radovanovic, J. Am. Chem. Soc. **132**(27), 9250 (2010).
[5]D. Machon, P. F. McMillan, B. Xu, and J. Dong, Phys. Rev. B **73**, 094125 (2006).
[6]Y. Xu, J. H. Park, Z. Yao, C. Wolverton, M. Razeghi, J. Wu, and V. P. Dravid, ACS Appl. Mater. Interfaces **11**, 5536 (2019).
[7]E. A. Anber, D. Foley, A. C. Lang, J. Nathaniel, J. L. Hart, M. J. Tadjer, K. D. Hobart, S. Pearton, and M. L. Taheri, Appl. Phys. Lett. **117**, 152101 (2020).
[8]F. Mezzadri, G. Calestani, F. Boschi, D. Delmonte, M. Bosi, and R. Fornari, Inorg. Chem. **55**, 12079 (2016).
[9]S. W. Kim, S. Iwamoto, and M. Inoue, Ceram. Int. **35**, 1603 (2009).
[10]J. Moloney, O. Tesh, M. Singh, J. W. Roberts, J. C. Jarman, L. C. Lee, T. N. Huq, J. Brister, S. Karboyan, M. Kuball, P. R. Chalker, R. A. Oliver, and F. C. P. Massabuau, J. Phys. D **52**, 475101 (2019).
[11]Y. S. Hsieh, C. Y. Li, C. M. Lin, N. F. Wang, J. V. Li, and M. P. Houng, Thin Solid Films **685**, 414 (2019).
[12]B. L. Aarseth, C. S. Granerød, A. Galeckas, A. Azarov, P. D. Nguyen, Ø. Prytz, and L. Vines, Nanotechnology **32**, 505707 (2021).
[13]A. Meldrum, R. F. Haglund, Jr., L. A. Boatner, and C. W. White, Adv. Mater. **13**, 1431 (2001).
[14]E. Wendler, E. Treiber, J. Baldauf, S. Wolf, and C. Ronning, Nucl. Instrum. Methods Phys. Res., Sect. B **379**, 85 (2016).
[15]A. Nikolskay, E. Okulich, D. Korolev, A. Stepanov, D. Nikolichev, A. Mikhaylov, D. Tetelbaum, A. Almaev, C. A. Bolzan, A. Buaczik, Jr., R. Giulian, P. L. Grande, A. Kumar, M. Kumar, and D. Gogova, J. Vac. Sci. Technol. A **39**, 030802 (2021).
[16]A. Azarov, C. Bazioti, V. Venkatachalapathy, P. Vajeeston, E. Monakhov, and A. Kuznetsov, Phys. Rev. Lett. **128**, 015704 (2022).
[17]K. E. Sickafus, H. Matzke, T. Hartmann, K. Yasuda, J. A. Valdez, P. Chodak III, M. Nastasi, and R. A. Verrall, J. Nucl. Mater. **274**, 66 (1999).
[18]G. Sattonnay and L. Thomé, J. Nucl. Mater. **348**, 223 (2006).
[19]A. Benyagoub, Phys. Rev. B **72**(9), 094114 (2005).
[20]A. Benyagoub, Nucl. Instrum. Methods Phys. Res., Sect. B **218**, 451 (2004).
[21]U. C. Bind, R. K. Dutta, G. K. Sekhon, K. L. Yadav, J. B. M. Krishna, R. Menon, and P. Y. Nabhiraj, Superlattices Microstruct. **84**, 24 (2015).
[22]S. Dhara, A. Datta, C. T. Wu, Z. H. Lan, K. H. Chen, Y. L. Wang, C. W. Hsu, C. H. Shen, L. C. Chen, and C. C. Chen, Appl. Phys. Lett. **84**, 5473 (2004).
[23]A. Manna, A. Barman, S. R. Joshi, B. Satpati, P. Dash, A. Chattaraj, S. K. Srivastava, P. K. Sahoo, A. Kanjilal, D. Kanjilal, and S. Varma, J. Appl. Phys. **124**, 155303 (2018).
[24]D. J. Sprouster, R. Giulian, C. S. Schnohr, L. L. Araujo, P. Kluth, A. P. Byrne, G. J. Foran, B. Johannessen, and M. C. Ridgway, Phys. Rev. B **80**(11), 115438 (2009).
[25]H. Y. Playford, A. C. Hannon, E. R. Barney, and R. I. Walton, Chem. Eur. J. **19**, 2803 (2013).
[26]V. Vasanthi, M. Kottaisamy, and V. Ramakrishnan, Ceram. Int. **45**, 2079 (2019).
[27]X. Zhang, Z. Zhang, J. Liang, Y. Zhou, Y. Tong, Y. Wang, and X. Wang, J. Mater. Chem. A **5**, 9702 (2017).
[28]Y. Teng, L. X. Song, A. Ponchel, Z. K. Yang, and J. Xia, Adv. Mater. **26**, 6238 (2014).

[29]T. Yoo, X. Xia, F. Ren, A. Jacobs, M. J. Tadjer, S. Pearton, and H. Kim, Appl. Phys. Lett. **121**, 072111 (2022).
[30]T. Oshima, K. Matsuyama, K. Yoshimatsu, and A. Ohtomo, J. Cryst. Growth **421**, 23 (2015).
[31]H. M. Jeon, K. D. Leedy, D. C. Look, C. S. Chang, D. A. Muller, S. C. Badescu, V. Vasilyev, J. L. Brown, A. J. Green, and K. D. Chabak, APL Mater. **9**, 101105 (2021).
[32]S. B. Kjeldby, A. Azarov, P. D. Nguyen, V. Venkatachalapathy, R. Mikšová, A. Macková, A. Kuznetsov, Ø. Prytz, and L. Vines, J. Appl. Phys. **131**, 125701 (2022).
[33]P. A. Stadelmann, see https://www.jems-swiss.ch/ for more information about the software used for SAED simulations.
[34]I. Cora, F. Mezzadri, F. Boschi, M. Bosi, M. Čaplovičová, G. Calestani, I. Dódony, B. Pécz, and R. Fornari, Cryst. Eng. Commun. **19**, 1509 (2017).
[35]I. Cora, Z. Fogarassy, R. Fornari, M. Bosi, A. Recnik, and B. Pécz, Acta Mater. **183**, 216 (2020).
[36]P. Castro-Fernandez, M. V. Blanco, R. Verel, E. Willinger, A. Fedorov, P. M. Abdala, and C. R. Müller, J. Phys. Chem. C **124**(37), 20578 (2020).
[37]P. Kalita, S. Saini, P. Rajput, S. N. Jha, D. Bhattacharyya, S. Ojha, D. K. Avasthi, S. Bhattacharya, and S. Ghosh, Phys. Chem. Chem. Phys. **21**, 22482 (2019).